Chinese Journal of Oceanology and Limnology
Vol. 34 No. 3, P. 608-618, 2016
http://dx.doi.org/10.1007/s00343-016-4388-7

Reversal process of the South China Sea western boundary current in autumn 2011*

ZHANG Zhixin (张志欣)[1, 2], GUO Jingsong (郭景松)[2, **], GUO Binghuo (郭炳火)[2]

[1] *College of Physical and Environmental Oceanography*, *Ocean University of China*, *Qingdao 266100*, *China*

[2] *Laboratory of Marine Science and Numerical Modeling*, *First Institute of Oceanography*, *State Oceanic Administration* (*SOA*), *Qingdao 266061*, *China*

Received Dec. 20, 2014; accepted in principle Feb. 14, 2015; accepted for publication Mar. 15, 2015

Abstract Using merged sea level anomaly and absolute geostrophic velocity products from satellite altimetry and Argos drifter data, we analyzed the reversal process of the South China Sea (SCS) western boundary current (SCSwbc) from a summer to winter pattern in 2011 and important oceanic phenomena during this process. Results show that the outbreak time of the northeast monsoon over the southern SCS lagged that over the northern SCS by about 1 month. During the SCS monsoon reversal period, the SCSwbc reversed rapidly into the winter pattern at the Guangdong continental slope in late September. Subsequently, the southward Vietnam coastal boundary current strengthened. However, the northward Natuna Current maintained a summer state until mid-October. Thus, the balance between the southward and northward currents was lost when they met, their junction moved gradually southward. However, a loop current formed southeast of Vietnam because the main stream of the Vietnam Offshore Current (VOC) remained near its original latitude. Meanwhile, the VOC and associated dipole circulation system strengthened. After mid-October, the northward Natuna Current began to weaken, the loop current finally shed, becoming a cool ring. The VOC and its associated dipole sub-basin circulation system also weakened gradually until it disappeared.

Keyword: South China Sea; western boundary current; reversal process; northeast monsoon

1 INTRODUCTION

The South China Sea (SCS) is the largest semi-enclosed marginal sea of the western Pacific Ocean, whose northern portion connects to the Pacific through the Luzon Strait. Its southern portion connects with the Indian Ocean through the Karimata Strait, Java Seas and several other straits. Topography of the SCS is complex, with a vast sea area of depths greater than 1 000 m and numerous islands, shoals and gulfs, as well as complex shorelines (Fig.1). Such unique features of the geography and topography affect dynamic characteristics of the SCS. These include a meridional circulation and variously sized eddies similar to the open ocean, and a strong seasonal circulation caused by monsoons, in contrast with the open ocean. The SCS circulation is generally a cyclonic gyre in winter and an anticyclonic gyre in summer (Hu et al., 2000) with multiple eddies (Hwang and Chen, 2000; Wang et al., 2003; Xiu et al., 2010; Chen et al., 2011; Chu et al., 2014). Among these circulations, a strong current with obvious seasonal variation appears along the SCS northern continental shelf and the Indochina east coast, called the South China Sea western boundary current (SCSwbc). The SCSwbc significantly influences seasonal transformation of the upper-layer circulation, heat transport, regional climate, and others. Wyrtki (1961) first pointed out the westward intensification of SCS circulation. Afterward, there have been substantial

* Supported by the UNESCO-IOC/WESTPAC Project "Response of marine hazards to climate change in the Western Pacific", the Special Fund of Chinese Central Government for Basic Scientific Research Operations in Commonweal Research Institutes (No. GY0212172), and the Open Foundation of the Key Laboratory of Data Analysis and Applications, State Oceanic Administration (No. LDAA-2012-02)
** Corresponding author: gjings23@fio.org.cn

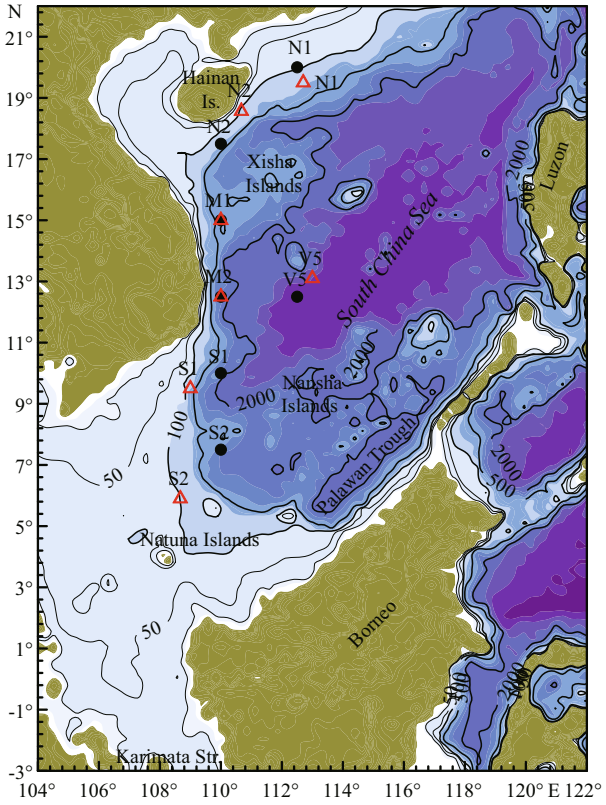

Fig.1 Topography of study areas

Black dots denote locations of representative stations for wind fields, and red triangles mark stations representative of geostrophic current. Topography is indicated by contour lines; unit: m.

investigations of the SCSwbc, such as its paths, state, volume transport, seasonal and inter-annual variation, as well as statistical features of its eddies. These researches have been based on in-situ observations, Argos drifter and satellite altimetry data, and numerical models (e.g., Li, 2002; Wu and Chang, 2005; Fang et al., 2006; Wang et al., 2013).

The SCSwbc is mainly driven by the monsoon (Liu et al., 2001; Yang et al., 2002; Cai et al., 2007; Liu et al., 2008a; Wang et al., 2010; Yang and Wu, 2012). The SCSwbc has two stable seasonal modes corresponding to the monsoon. In winter, the SCSwbc moves westward along Guangdong continental slope, turns southward off Hainan Island, and then flows southward along the Vietnam coast, arriving near the Natuna Islands. The SCSwbc separates into two branches here. One branch continues to flow southward towards the Java Sea through the Karimata Strait. The other turns eastward and forms a cyclonic gyre (Fang et al., 1998; Shaw et al., 1999; Hu et al., 2000; Li et al., 2000; Fang et al., 2005; Liu et al., 2008b; Fang et al., 2012). In summer, SCSwbc structure is very complex, it starts from the Karimata Strait and flows northward in June. When this boundary current reaches the area around 11°N, it turns eastward to form the Vietnam Offshore Current (VOC) (Shaw and Chao, 1994; Fang et al., 1998; Takano et al., 1998; Ho et al., 2000; Fang et al., 2002, 2006; Liu et al., 2008b). Meanwhile, a dipole circulation forms on both sides of the VOC (Wang et al., 2006), a stable sub-basin-scale anticyclonic gyre appears on the south side and a cyclonic gyre on the north side. The circulation structure is very complex at the northern continental shelf of the SCS, especially near the Dongsha Islands.

The seasonal difference or current states of the SCSwbc during seasonal transition have been mainly studied based on data of monthly averages or certain periods (Fang et al., 2002, 2006; Liu et al., 2008b). However, studies on the seasonal transition processes of the SCSwbc circulation patterns are still relatively few. In particular, important phenomena related with the transition processes have not been much studied. In this paper, the reversal process of the SCSwbc from a summer to winter pattern is illustrated in detail, based on satellite altimetry products and Argos drifting buoy data. Further, important oceanic phenomena during this reversal process are described.

2 DATA

For studying the reversal process of the SCSwbc in autumn, we collected merged altimeter-based daily sea level anomaly (MSLA) data with resolution 0.25°×0.25° and absolute geostrophic velocity products with resolution 0.33°×0.33° from July–December 2011 over the SCS. These data were from Archiving, Validation and Interpretation of Satellite Oceanographic (AVISO). The MSLA and geostrophic flow data products from AVISO are widely used in the study of mesoscale eddies in the SCS. We also used 2011 daily average surface wind data with resolution of 2.5°×2.5°, provided by the National Centers for Environmental Prediction/National for Atmospheric Research (NCEP/NCAR). To investigate the relationship between geostrophic flow and wind, the selected NCEP reanalysis data were nearest-neighbor and synchronous with AVISO.

Argos drifter data from the NOAA Atlantic Oceanographic and Meteorological Laboratory are also used. We found 15 drifters within the study area for autumn. The available drifters were from the period 2004–2011. Among these, 80% were north of 16°N and some continued operation during summer, autumn and winter.

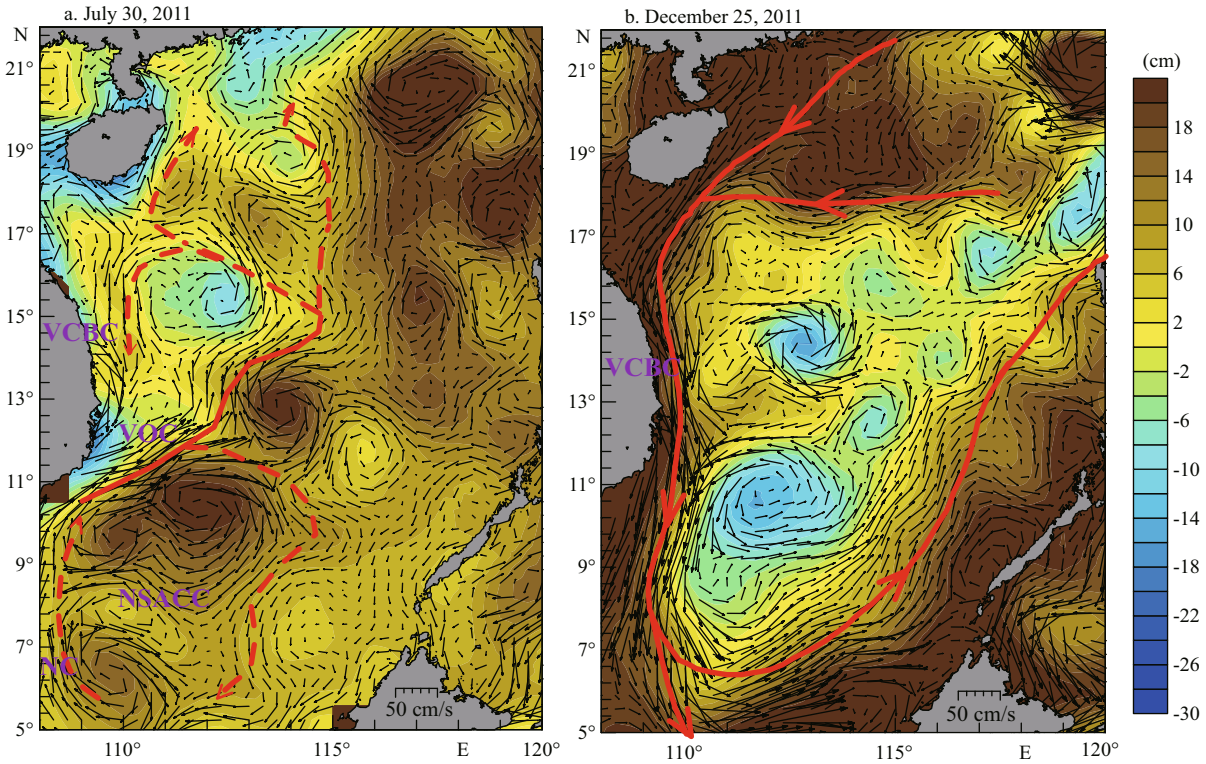

Fig.2 Maps of merged absolute geostrophic velocities and merged sea level anomalies in SCS during summer (a) and winter (b) 2011

Red lines mark most significant circulation systems in SCS during summer and winter 2011. VCBC, VOC, NC and NSACC in Fig.2 indicate Vietnam Coastal Boundary Current, Vietnam Offshore Current, Natuna Current and Nansha anticyclonic circulation, respectively.

3 BASIC FEATURES OF THE CIRCULATIONS IN WINTER AND SUMMER

To analyze the SCSwbc reversal process from the summer to winter pattern, we first briefly describe basic features of SCS circulations in those two seasons, based on absolute geostrophic current and MSLA fields on July 30, 2011 and December 25, 2011 (Fig.2). Figure 2b clearly shows that a single cyclonic basin-scale circulation emerged in the SCS during winter. Under driving of the northeast monsoon, one current moved southward along the western boundary with a narrow breadth and large velocity. A northward current near the eastern boundary is associated with a compensation current, which flowed northward with large breadth and small velocity. Its main current zone south of 11°N was not close to the SCS eastern boundary, but was in the area west of the Palawan Trough. In the interior of the sea-basin circulation, there were two strong current zones north of 17°N. One moved along the western boundary. The other flowed westward from the southern Luzon Strait area, and began to turn southwestward and converged with the western boundary current upon arrival in the area north of the Xisha Islands. In the area between the two strong currents, anticyclonic eddies were stronger than cyclonic ones. However, the latter prevailed in the interior circulation south of 17°N.

Figure 2a shows a distinct circulation system (marked by red line) in summer, although there were very active mesoscale eddies across the entire SCS. Within this system, a most important current was the well-known VOC. Fang et al. (2012) indicated that this flow originates from the SCSwbc. The summer SCSwbc starts from the Karimata Strait and flows northward along the southern Malay Peninsula, then passes by the mouth of the Gulf of Thailand and flows northeastward along the southeastern Vietnamese coast. When this current reaches the area at 11°N, it turns eastward to form the offshore current called the VOC. Figure 2a clearly shows that a northward current appeared at the SCS outer edge of the southwest continental shelf, which is called the Natuna Current because of its passage through the area near the Natuna Islands. The upper part of that current comes from the Karimata Strait and has depth less than 50 m (Fig.1), but currents in the middle and

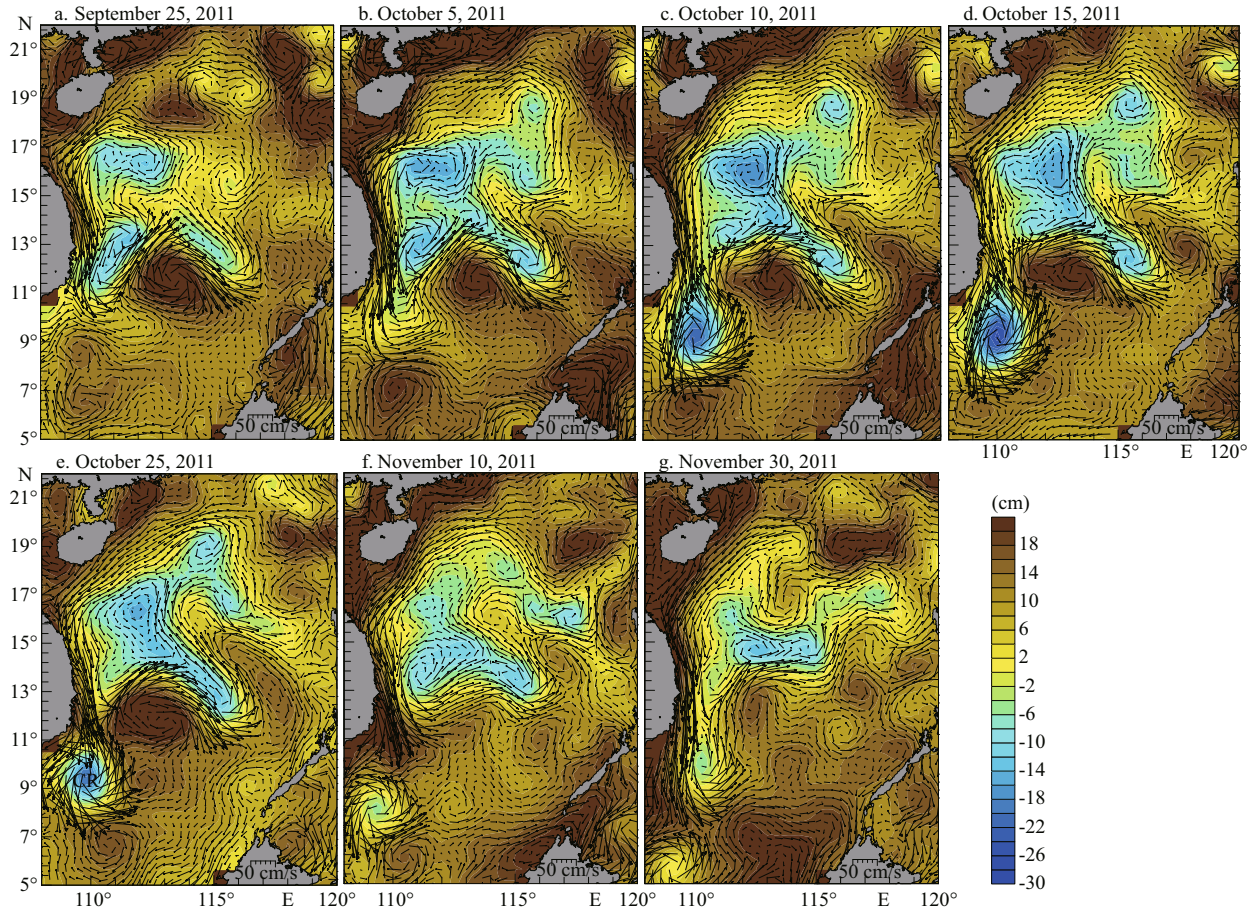

Fig.3 Maps of merged sea level anomaly (cm) and merged absolute geostrophic velocities in SCS during September 25–November 30, 2011

CR represents cyclonic current ring.

deep layers may be an inner flow in the southern SCS. The Natuna Current moved away from the continental slope to the southeast of Vietnam (10°N, 109°E) and then turned northeast to become the VOC. It was the strongest current in the SCS circulation during summer, with maximum velocity 1 m/s. The VOC had a strikingly meandering path accompanied by a number of mesoscale eddies and several branch. The first branch appeared around 12°N, 112°E. This branch flowed southeastward, then turned back clockwise to its origin area, and ultimately forming an anticyclonic circulation referred to as the Nansha anticyclonic circulation (Li, 2002). Its main stream continued to flow northward and appeared another branch around 15°N, 115°E. However, the speed of this branching current was weak, so it was considered an extension of the VOC. A branch of this extension current turned northward and directly reached the SCS northern continental slope region. Another branch turned northwestward and branched again around 17°N, 111°E; one of those branches turned northward to flow along the eastern coast of Hainan Island, then turned northeastward along the SCS northern continental slope to converge with the branch flowing straight northward. The other branch turned southward to flow along the eastern coast of southern Vietnam (referred to as the Vietnam Coastal Boundary Current or VCBC). A part of the extension current constituted a cyclonic sub-basin-scale circulation together with the main stream of the VOC. This cyclonic and anticyclonic circulations south of the VOC formed a dipole circulation (Wang et al., 2006). This was readily discerned by combining MSLA maps in which the sea-surface height near the center of cyclonic circulation was ~15 cm lower than surrounding heights. However, the anticyclonic circulation south of the VOC showed the westward intensification similar to the open sea circulation.

4 REVERSAL PROCESS OF THE SCSWBC IN AUTUMN

According to the above analyses for the summer circulation, daily absolute geostrophic current and sea level anomaly maps of the SCS (Fig.3), we divided

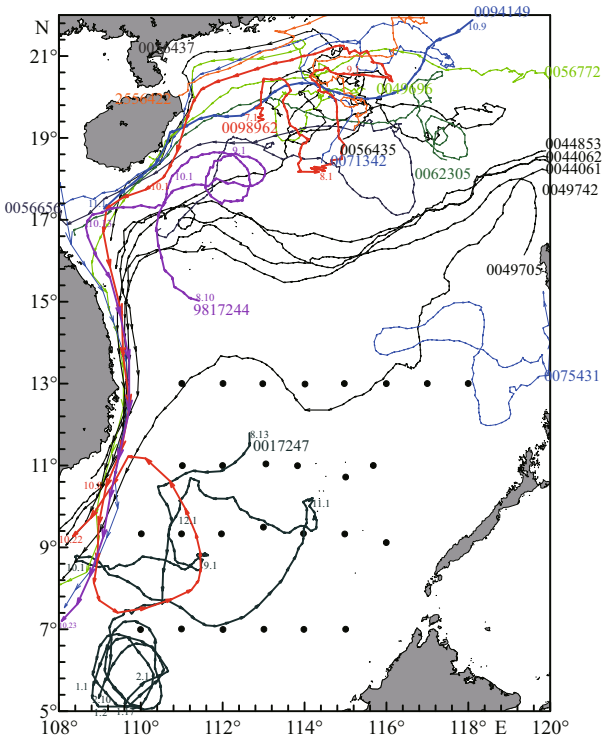

Fig.4 Daily displacement trajectories of Argos drifters

Digits denote date (month/day) that the drifters reached indicated locations.

the SCS into north, middle and south portions. The northern portion is north of 17°N, where the SCSwbc begins from the southeast of Hainan Island across all the Guangdong continental slope. The middle portion is between 11°–17°N, where the VCBC, VOC and sub-basin-scale cyclonic circulation are found. The southern portion is south of 11°N, containing the Natuna Current and Nansha anticyclonic circulation.

4.1 Northern portion

The above analyses show that the western boundary current driven by the southwest monsoon flowed northeastward along the Guangdong continental slope during summer. This current pattern persisted until mid–September. Figure 3 shows that a southwestward current with velocities of 20–40 cm/s (Fig.3b–e) had formed at the Guangdong-Hainan continental slope after September 25. Surface geostrophic currents converged westward into the western boundary current in areas north of 17°N and west of 117°E. This convergent trend strengthened gradually, which greatly enhanced the western boundary current during October 5 through 25 (Fig.3b–e). Multiple-eddy regions were east of 117°E, and the relationship between the SCSwbc and eddies was complicated. After October 25 the convergent trend decreased and the range of the stable west-southwestward current gradually returned to west of 114°E.

4.2 Middle portion

The VOC and its associated cyclonic circulation occupied most of the middle portion (i.e., 11°–17°N and west of 115.5°E) in summer (Fig.2a), and the two greatly strengthened in autumn (Fig.3). We provide more detail on this situation as follows. The VCBC first strengthened after September 25, perhaps because the western boundary current of the northern portion entered the Vietnam coastal region from the north. Figures 4 and 5 show that velocities of the VCBC increased from about 20 cm/s to 40–60 cm/s at station M1 and about 30 cm/s to 60–90 cm/s at station M2 after September 24, respectively. This implies that the VCBC was already dominated by the monsoon current and became a part of the SCSwbc winter pattern. The VCBC flowing southward along the coast met the northward Natuna Current around 10.5°N, and then the both flowed eastward together to form the VOC, which was strengthened remarkably. There were some accompanying dynamic phenomena, such as the VOC turning eastward from northeastward, the cyclonic circulation system strengthening and extending eastward to ~117°E. Curvatures of the meandering path of this system increased, and mesoscale cold eddies in its interior increased in number and strength. In contrast with summer, the maximum decline of sea level in the circulation interior was not at its center, but at centers of some cold eddies. This implies that upwelling caused by the eddy was much stronger than that by a sub-basin circulation with sufficiently strong current. Figure 3d shows that this developing trend peaked around October 15. Afterward, the northward Natuna current gradually weakened, so the southward VCBC advanced southward and reduced transport into the VOC. Meanwhile, this circulation system and the accompanying mesoscale phenomena also gradually weakened. At the end of November, the VOC was only supported by the VCBC. The northward extent of the cyclonic circulation system shrank to areas between 13°N and 17°N during this period. In December, the VOC completely lost its sources and disappeared (Fig.2b).

4.3 Southern portion

Figure 3 demonstrates that current structures south of the VOC after October 5 maintained basic features similar to those of the anticyclonic sub-basin

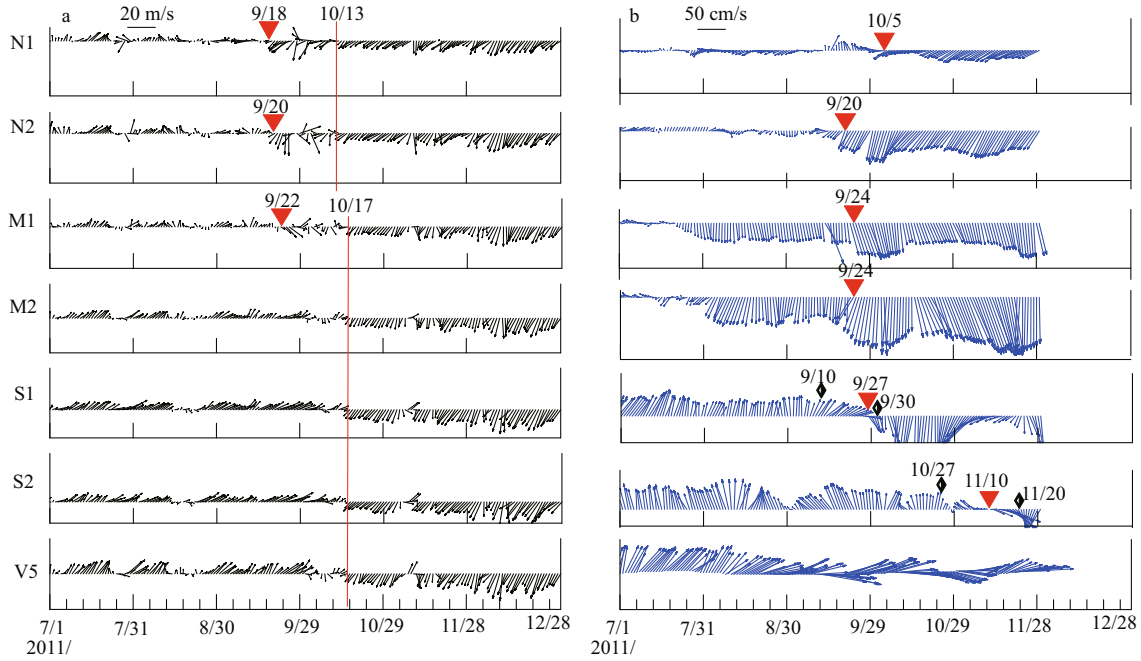

Fig.5 a. time series of reanalyzed sea surface wind vectors from NCEP/NCAR; b. surface geostrophic flow vectors from AVISO at seven stations representative of SCSwbc

circulation in summer. That is: (1) the westward intensification center of the anticyclonic circulation close to the SCS southwest continental shelf was very stable, which persisted through the end of October, but the sub-basin circulation was already unclear on November 10 (Fig.3f); (2) the anticyclonic (warm) eddy at the first rightward bend of the VOC was continuous through the end of October. Comparison of Figs.3a–e and 2a indicates that this autumn warm eddy was much stronger than in summer.

In the southern SCS a spectacular phenomenon was the appearance of a current ring with a cold water at its center (referred to as a cold ring) southeast of Vietnam. Its generation and dissipation are described as follows. After the onset of the northeast monsoon in the southern SCS, the convergent point of the VCBC and Natuna Current advanced southward because the former intensified and the latter weakened. Meanwhile, the VOC maintained its original position, so a meandering current appeared southeast of Vietnam (Fig.3a) on September 25, then arrived at ~8°N to form a loop current on October 5. Because a submarine ridge with depth <500 m near 8°N, 110°E intruded into the deep water area, the vanguard of the loop current was obstructed and persisted temporarily. The loop current nearly closed on October 10 (Fig.3c). This closed completely on October 25 (Fig.3e) and formed a cyclonic cold ring with center at 9.4°N, 110°E. The diameter of this cold ring was ~250 km with speed 1 m/s and the sea level height anomaly at its center was about 20 cm lower than at its margin. The cold ring separated fully from the VCBC and VOC on October 25, then crossed the submarine ridge and moved slowly southward at 8 cm/s. The cold ring shrank and greatly weakened through November 10, when its center moved southward to around 8°N, 105°E. On November 30 the ring diameter decreased to 200 km and its center reached near 5.5°N, 109.2°E. The trajectory of Argos drifter No. 0098962 (red line in Fig.4) reveals the existence of the cold ring. This drifter moved and reached east of Hainan Island on July 1, 2011 and entered the western boundary current in the northern SCS, then proceeded southward along the western boundary, finally entering an anticlockwise circulation centered near 9°N, 110°E. This circulation had a diameter ~250 km and a rotation speeds 50–150 cm/s. This observation is consistent with the occurring period, position, scale and rotating velocity of the cold ring shown in Fig.3c–e.

We also see in Fig.3e and f that there were two important variations after formation separation of the cold ring on October 25: (1) the northward current was replaced by the cold ring at the continental slope south of 7°N (station S2 in Fig.5). The VOC lost support from the Natuna current and the VCBC became its sole source, so the VOC weakened rapidly; (2) after the cold ring traversed the submarine ridge, the VCBC moved southward and formed another loop

Table 1 Characteristic quantities of turn direction (or transfer pattern) for Argos drifter trajectories in northern SCS

Drifter number	Starting and ending times (Year/month/date)	Date (Month/day)	Coordinates	V_b, V_a
9817244	00/8/10–10/23	9/22	112.2°E, 18.6°N	23, 24
2556422*	05/7/1–10/16	9/16–25	114.5°E, 22.0°N	16, 27
0056437	05/7/1–10/12	9/21	114.2°E, 21.7°N	12, 42
0049696	05/7/1–06/1/2	9/22	114.0°E, 21.2°N	20, 60
0071342	07/7/1–11/13	9/17	116.3°E, 21.8°N	24, 36
0098962	11/7/1–10/23	9/18	114.9°E, 21.2°N	31, 55
0056656	06/7/1–10/3	9/12	115.2°E, 19.2°N	22, 46
0062305*	06/7/1–9/29	8/22	116.0°E, 19.4°N	15, 25
0056435*	05/7/1–12/8	10/10	117.5°E, 19.4°N	26, 27
0056772	05/9/17–11/8	/	/	/, /
0094149	09/10/9–11/1	Southwestward		60, 60
0044853	04/10/7–05/1/23	Westward before 12/1		/
0044062	04/10/5–12/16			/
0044061	04/10/5–12/6			/
0049705	04/10/13–12/26			/

V_b and V_a denote mean speeds during 10 days before and after transfer direction; unit: cm/s; V_b and V_a of drifter No. 2556422 were taken as mean speeds before September 16 and after September 25, respectively, because of data loss during September 16–25; * denotes transition of drifter trajectories from stable directions to circle pattern.

current in the same area. This current was much weaker than the former because of the lack of support from the northward Natuna current. Sea level of the southern part of this current (centered at ~10°N, 110.5°E) was lowest, which heralds formation of a new cold ring; (3) the cold ring obstructed southward advance of the VCBC, and establishment of the winter pattern circulation structure was therefore postponed in the southern SCS. The trajectory of drifter No. 0017247 deployed on August 3, 2000 (dark green line in Fig.4), clearly displays a cyclonic eddy. This eddy rotated counterclockwise around a center at 6°N, 110°E from mid-December 2000 through mid-February, with speed 60 cm/s and diameter ~220 km. However, the appearance of this eddy was more than 1 month later than the cold ring in Fig.3. We suspect that the eddy formed during autumn of the preceding year.

4.4 Response of SCSwbc to northeast monsoon

4.4.1 Response of surface current

To further analyze the response of the SCSwbc to the northeast monsoon, we first found 15 drifters that were deployed or entered the SCS during summer and autumn, then plotted their daily trajectories (Fig.4). Trajectory starting points shown in Fig.4 are the drifter deployment dates. If the drifters were deployed before July 1, starting dates are given as July 1. The 15 drifters were roughly divided into three groups, based on variations of SCS surface circulation shown in Fig.4 and Table 1. The first group includes six drifters (0056437, 0049696, 2556422, 0098962, 9817244 and 0071342), the second seven, and the third two.

The first group of drifters moved west of 117°E in the northern SCS before mid-September, whose trajectories are shown by circles of different sizes in Fig.4. This implies that this area is one of active eddies. Put another way, eddy currents were much stronger than the mean current. Table 1 shows that drifter 9817244 turned westward from northward at 18.6°N, 112.2°E, then southwestward and westward again during September 17–22. It converged with the VCBC on October 13. The other five drifters of the first group turned southwestward along the Guangdong continental slope at 21.2°–22°N to form the SCSwbc winter pattern. Their mean speeds during 10 days were 27–60 cm/s after turning in direction, 1.5–3 times those before this turn. Drifter 0098962 data shown in Table 1 and the reanalyzed surface wind fields shown in Fig.5 were from the same period in 2011, which show that both of the turning directions of the current and the wind occurred on September 18. Thus, it is seen that response of the surface Ekman current to the northeast monsoon was not delayed

obviously. Although the six drifters in the northern SCS were deployed in four years, their turning directions all took place around September 20 because of the northeast monsoon. Moreover, the surface Kuroshio branch from the Luzon Strait had already formed by mid and late September (Guo et al., 2012) and joined the western boundary current flowing southwestward along the Guangdong continental slope in the northern SCS during winter.

Among the seven drifters in the second group, numbers 0044853, 0044062 and 0044061 entered the SCS from the Luzon Strait during the first 10 days of October, then traversed the northern SCS from east to west with mean speed 20 cm/s. The drifters arrived in the Xisha region through early December, then joined the southward western boundary current. Drifter 0049705 flowed northward along the Luzon Island western coast, then joined that current. Drifters 0056772 and 0094149 crossed 118°E from southwest of Taiwan Island in early October 2005 and 2009, respectively. They moved westward, then arrived to the east of Hainan Island on November 2 and October 26, respectively. Drifter 0056435 traced an irregular curve or circled before October 10, then moved westward stably from about 117.6°N, 19.4°E, turned southwestward on November 3, finally joining the western boundary current on January 2.

Observations from two groups of drifters show that mesoscale eddies were very active in the northern SCS during summer and dominated the surface current field. The surface current turned rapidly southwestward around the Guangdong continental slope with onset of the northeast monsoon around September 20, then surface water began to converge westward. The surface circulation fully transitioned into the winter pattern by early October. Except for the northward current off the west coast of Luzon Island, the surface water moved consistently westward in the northern SCS, forming the SCSwbc winter pattern. In this period, a stable northeast current caused by the monsoon was dominant, although mesoscale eddies remained active in the area.

Two drifters of the third group were deployed before July 1, 2006. Drifter 0062305 circled east of 116°E before August 22, then moved straight westward with small mean speed (only 25 cm/s in the first 10 days). Its speed increased ~50 cm/s upon arriving east of Hainan Island. Drifter 0056656 circled east of 115.2°E before September 12, moved westward steadily from around 115.2°E, 19.2°N with mean speed 51 cm/s in the first 10 days, and turned southwestward off Hainan Island through September 21. This indicates that the appearance of the westward surface current in 2006 was earlier than in normal years. The westward trajectories of the two drifters were similar, but there was one times speed difference of their moving speed. The westward current measured by drifter 0056656 had mean speed ~50 cm/s from September 12, which was considered a northeast monsoon current. There was clear westward surface currents revealed by drifter 0062305 from August 22, with mean speed only ~25 cm/s. These are considered currents prior to onset of the northeast monsoon. These currents possibly resulted from northwestward extension of the sub-basin cyclonic circulation to the middle portion. Reversal of the SCS surface current in summer-autumn 2006 was abnormal, possibly related to a weak El Niño in this year.

4.4.2 Response of geostrophic current

We selected seven representative stations of the SCSwbc (Fig.1) and plotted their time series of wind and current (Fig.5) based on absolute geostrophic flow data from AVISO and surface wind data from NCEP/NCAR. Responses of the geostrophic current to the monsoon were analyzed. Stations N1 and N2 were at the Guangdong continental shelf and off the Hainan Island coast, respectively. Figure 5 shows that the prevailing south-southwest wind was very weak at the two stations in summer, and that over station N1 was weaker than over N2. Geostrophic currents at the two stations were less than 10 cm/s mostly with unstable directions. This implies that the northeastward large-scale mean current at the continental slope was not dominant in the geostrophic current field during summer, and that the mesoscale eddy current was stronger than the large-scale mean current. The response of the geostrophic current to the monsoon varied between the two stations. The monsoon over station N1 changed rapidly into a northeast monsoon on September 18, and drifter 0098962 turned immediately southwestward near that station. Its mean speeds reached 55 cm/s in the first 10 days after turning direction (Table 1). However, Figs.3 and 5 show that the stable southwestward geostrophic current at N1 occurred after October 5. Its mean speed was ~10 cm/s in the first few days and increased to 20 cm/s after October 20. This indicates that the stable southwestward geostrophic current along the Guangdong continental shelf slope lagged the directional turn of the surface current indicated by the

Argos drifters by ~15 days. At station N2, the northeast monsoon began on September 18, where the original southward geostrophic current suddenly intensified, with speed from 15 to 40 cm/s. Obviously, responses of the geostrophic current to the northeast monsoon varied substantially between the two stations, which may be related to different current fields before monsoon outbreak.

Figure 5 shows that southward wind over station M1 persisted untill September 22. The monsoon reversal period was September 26–October 15. Northward wind during this period was already dominant. Southward wind at station M2 persisted through October 17 with speeds slightly greater than at M1. Currents at the two stations maintained a stable southward direction after July 31 with speeds 20 and 30 cm/s, respectively. Obviously, the VCBC characterized by the currents at the two stations was indirectly related to the local southwestward monsoon. Variation of these current were consistent. The VCBC clearly strengthened with speeds 30–40 cm/s at station M1 after September 24 owing to joining of the western boundary current from the northern portion. Speeds (~50–100 cm/s) clearly increased more at station M2, owing to narrowing of the current width.

Stations S1 and S2 were at the southwest continental shelf slope of the SCS. S1 was around the initiating location of the VOC. The southwest monsoon was in control at S1 before October 17, and wind speeds were slightly stronger than at Station M2. Afterward, the northeast monsoon was in control. A northward current ~30 cm/s at S1 persisted until September 10, and then turned eastward again to the southward. After September 30, the current turned into a stable southward flow. Its speed increased to ~80 cm/s. In November, however, its speed showed great variation from strong to weak and back to strong. The above analyses illustrate that the variations of dominant currents at this station were VOC → current loop → cold ring. Obviously, these variations did not fully depend on the local northeast monsoon. The northward current at station S2 persisted through October 27. Afterward, the current direction changed gradually clockwise from north to south, and its speed varied from strong to zero and back to strong. After November 20, a steady southward current with speed ~15 cm/s persisted at Station S2.

Station V5 was in the VOC (Figs.1 and 3). One sees in Fig.5 that northeast monsoon onset over this station was around October 15, the same as over S1 and S2. However, the current at Station V5 representing the VOC flowed northeastward before August 22, and then turned gradually eastward. Clearly, the VOC did not directly respond to the monsoon reversal.

The above analyses show that the reversal times of the geostrophic component of the SCSwbc at the Guangdong continental slope and southwest continental slope of the SCS lagged the monsoon reversal in the two areas by about 15 and 25 days, respectively. However, variations of the VCBC and VOC were not directly related to the local monsoon. Specifically, the northeast monsoon over the SCS began to form about September 20 in the northern portion, and then developed gradually southward, occupying the entire SCS through mid-October. The surface and geostrophic currents were not synchronous in their response to the monsoon. That response of the surface current was not greatly delayed at the Guangdong continental slope, but the southwestward geostrophic current was delayed by ~15 days. At station S2 in the southern portion, the monsoon direction reversed on October 17, whereas the direction of the geostrophic current changed on November 10. This means that the geostrophic current reversal was 23 days later than the monsoon. Regarding the geostrophic current in the middle portion, the VCBC remained stable with a southward direction, and the VOC direction varied only slightly from eastward from the end of August through end of November.

Surface current data from the Argos drifters contain Ekman current and geostrophic current components. Upon northeast monsoon onset, the surface Ekman current occurs immediately and causes adjustments of sea surface height, current and density fields. The geostrophic adjustment clearly begins from the original current fields, so the duration of that adjustment is related to both wind and the original current field. Moreover, the large-scale geostrophic current with stable direction appears only when speeds of the basin or sub-basin circulations exceed the rotational speed of mesoscale eddies.

5 CONCLUSION

We focused our analyses on the reversal process of the SCSwbc from a summer to winter pattern in 2011 and major associated oceanic phenomena, based on daily merged sea level anomalies, absolute geostrophic current products, and Argos drifter data. The principal results are as follows.

(1) The SCS surface current field is complex in summer. In the northern SCS (north of 17°N),

northeastward western boundary currents were often accompanied by mesoscale eddies. In the middle and southern SCS (south of 17°N), the basic circulation system was distinct. This system included the VOC and associated dipole circulations constituted by an anticyclonic and cyclonic gyre south and north of the VOC, respectively. In winter, a single basin-scale cyclonic circulation appeared in the SCS.

(2) Onset of the northeast monsoon over the northern SCS was around September 20, which then advanced progressively to the southern SCS. This process lasted nearly 1 month. Two significant oceanic phenomena appeared during this period: a) the southward VCBC intensified noticeably and the Natuna Current maintained a northward flow, thereby strengthening the VOC and its dipole circulation system; b) as the VCBC and Natuna Current joined, the balance between the two currents was lost owing to the VCBC enhancement, and their juncture translated gradually southward. The main stream of the VOC remained near its original longitude. These two phenomena resulted in formation of a loop current. With the continued southward advance of the VCBC and Natuna Current weakening, this loop current detached and became a shedding cold ring in mid-October. Meanwhile, the VOC and its associated circulation system also decayed, and the SCS circulations fully transitioned to the winter pattern.

(3) The results show that SCSwbc responses to the monsoon in the three portions varied in autumn. At the Guangdong continental slope, the surface current and monsoon changed their directions nearly simultaneously, because the current fields were very weak in summer. The surface current was clearly dominated by the Ekman current in the early days after the change of current direction. This current lasted about 15 days to achieve geostrophic adjustment, and the dominant component changed from mesoscale eddies into sub-basin circulations. At the southwestern continental slope of the SCS, the turn direction of the currents proceeded from north to south. This was related not only to the monsoon, but also to the complex southward advance of the VCBC. In the middle portion, responses of the VCBC and VOC to the monsoon were unclear, and their variations depended on the western boundary current in the northern and southern portion.

References

Cai S Q, Long X M, Wang S A. 2007. A model study of the summer Southeast Vietnam Offshore Current in the southern South China Sea. *Cont*. *Shelf Res*., **27**(18): 2 357-2 372.

Chen G X, Hou Y J, Chu X Q. 2011. Mesoscale eddies in the South China Sea: mean properties, spatiotemporal variability, and impact on thermohaline structure. *J*. *Geophys*. *Res*., **116**(C6): C06018, http://dx.doi.org/10.1029/2010JC006716.

Chu X Q, Xue H J, Qi Y Q, Chen G X, Mao Q W, Wang D X, Chai F. 2014. An exceptional anticyclonic eddy in the South China Sea in 2010. *J*. *Geophys*. *Res*. *Oceans*, **119**(2): 881-897, http://dx.doi.org/10.1002/2013JC009314.

Fang G H, Fang W D, Fang Y, Wang K. 1998. A survey of studies on the South China Sea upper ocean circulation. *Acta Oceanographica Taiwanica*, **37**(1): 1-16.

Fang G H, Susanto D, Soesilo I, Zheng Q A, Qiao F L, Wei Z X. 2005. A note on the South China Sea shallow interocean circulation. *Advances in Atmospheric Sciences*, **22**(6): 946-954.

Fang G H, Wang G, Fang Y, Fang W D. 2012. A review on the South China Sea western boundary current. *Acta Oceanol*. *Sin*., **31**(5): 1-10.

Fang W D, Fang G H, Shi P, Huang Q Z, Xie Q. 2002. Seasonal structures of upper layer circulation in the southern South China Sea from in situ observations. *J*. *Geophys*. *Res*., **107**(C11): 3 202, http://dx.doi.org/10.1029/2002JC001343.

Fang W D, Guo J J, Shi P, Mao Q W. 2006. Low frequency variability of South China Sea surface circulation from 11 years of satellite altimeter data. *Geophys*. *Res*. *Lett*., **33**: L22612, http://dx.doi.org/10.1029/2006GL027431.

Fang W D, Guo Z X, Huang Y T. 1998. Observational study of the circulation in the southern South China Sea. *Chinese Science Bulletin*, **43**(11): 898-905.

Guo J S, Chen X Y, Sprintall J, Guo B H, Qiao F L, Yuan Y L. 2012. Surface inflow into the South China Sea through the Luzon Strait in winter. *Chinese Journal of Oceanology and Limnology*, **30**(1): 163-168.

Ho C R, Kuo N J, Zheng Q A, Soong Y S. 2000. Dynamically active areas in the South China Sea detected from TOPEX/POSEIDON satellite altimeter data. *Remote Sens*. *Environ*., **71**: 320-328.

Hu J Y, Kawamura H, Hong H S, Qi Y Q. 2000. A review on the currents in the South China Sea: seasonal circulation, South China Sea warm current and Kuroshio intrusion. *J*. *Oceanogr*., **56**(6): 607-624.

Hwang C, Chen S A. 2000. Circulations and eddies over the South China Sea derived from TOPEX/Poseidon altimetry. *J*. *Geophys*. *Res*., **105**(C10): 23 943-23 965.

Li L, Wu R S, Guo X G. 2000. Seasonal circulation in the South China Sea a TOPEX/POSEIDON satellite altimetry study. *Acta Oceanologica Sinica*, **22**(6): 13-26. (in Chinese with English abstract)

Li L. 2002. Advance in observational studies of upper layer circulations of the South China Sea. *Journal of Oceanography in Taiwan Strait*, **21**(1): 114-125. (in Chinese with English abstract)

Liu Q Y, Kaneko A, Su J L. 2008a. Recent progress in studies of the South China Sea circulation. *J*. *Oceanogr*., **64**(5):

753-762.

Liu Y G, Weisberg R H, Yuan Y C. 2008b. Patterns of upper layer circulation variability in the South China Sea from satellite altimetry using the self-organizing map. *Acta Oceanologica Sinica*, **27**(Suppl.): 129-144.

Liu Z Y, Yang H J, Liu Q Y. 2001. Regional dynamics of seasonal variability in the South China Sea. *J. Phys. Oceanogr*., **31**(1): 272-284.

Shaw P T, Chao S Y, Fu L L. 1999. Sea surface height variations in the South China Sea from satellite altimetry. *Oceanologica Acta*, **22**(1): 1-17.

Shaw P T, Chao S Y. 1994. Surface circulation in the South China Sea. *Deep Sea Res. I: Oceanogr. Res. Paper*., **41**: 1 663-1 683.

Takano K, Harashima A, Namba T. 1998. A numerical simulation of the circulation in the South China Sea-preliminary results. *Acta Oceanographica Taiwanica*, **37**(2): 165-186.

Wang D X, Hong B, Gan J P, Xu H Z. 2010. Numerical investigation on propulsion of the counter-wind current in the northern South China Sea in winter. *Deep Sea Res. I: Oceanogr. Res. Paper*., **57**(10): 1 206-1 221.

Wang D X, Liu Q Y, Xie Q, He Z G, Zhuang W, Shu Y Q, Xiao X J, Hong B, Wu X Y, Sui D D. 2013. Progress of regional oceanography study associated with western boundary current in the South China Sea. *Chinese Science Bulletin*, **58**(11): 1 205-1 215.

Wang G H, Chen D K, Su J L. 2006. Generation and life cycle of the dipole in the South China Sea summer circulation. *J. Geophys. Res*., **111**(C6): C06002, http://dx.doi.org/10.1029/2005JC003314.

Wang G H, Su J L, Chu P C. 2003. Mesoscale eddies in the South China Sea observed with altimeter data. *Geophys. Res. Lett*., **30**(21), http://dx.doi.org/10.1029/ 2003GL018532.

Wu C R, Chang C -W J. 2005. Interannual variability of the South China Sea in a data assimilation model. *Geophys. Res. Lett*., **32**(17): L17611, http://dx.doi.org/10.1029/ 2005GL023798.

Wyrtki K. 1961. Physical oceanography of the Southeast Asian waters. *In*: NAGA Report Volume 2. Scientific Results of Marine Investigations of the South China Sea and the Gulf of Thailand, S.I.O. La Jolla, California. 195p.

Xiu P, Chai F, Shi L, Xue H J, Chao Y. 2010. A census of eddy activities in the South China Sea during 1993-2007. *J. Geophys. Res*., **115**: C03012, http://dx.doi.org/10.1029/ 2009JC005657.

Yang H J, Liu Q Y, Liu Z Y, Wang D X, Liu X B. 2002. A General circulation model study of the dynamics of the upper ocean circulation of the South China Sea. *J. Geophys. Res*., **107**(C7): 3 085, http://dx.doi.org/10.1029/ 2001JC001084.

Yang H Y, Wu L X. 2012. Trends of upper-layer circulation in the South China Sea during 1959-2008. *J. Geophys. Res*., **117**: C08037, http://dx.doi.org/10.1029/2012JC008068.